

# Mapping the Thermal Lithosphere and Melting across the Continental US

Ryan C Porter<sup>1</sup> and Mary R. Reid<sup>1</sup>

<sup>1</sup>Northern Arizona University

November 21, 2022

## Abstract

The thermal regime of continental lithosphere plays a fundamental role in controlling the behavior of tectonic plates. In this work, we assess the thermal state of the North American upper mantle by combining shear-wave velocity models calculated using data from the EarthScope facility with empirically-derived anelasticity models and basalt thermobarometry. We estimate the depth to the thermal lithosphere-asthenosphere boundary (LAB), defined as the intersection of a geotherm with the 1300° C adiabat. Results show lithospheric thicknesses across the contiguous US vary between ~40 km and > 200 km. The thinnest thermal lithosphere is observed in the tectonically active western US and the thickest lithosphere in the mid-continent. By combining geotherm estimates with solidus curves for peridotite, we show that a pervasive partial melt zone is common within the western US upper mantle and that partial melt is absent in the eastern and central US without significant metasomatism.

# 1 Mapping the Thermal Lithosphere and Melting across the 2 Continental US

3 Ryan Porter<sup>1</sup>; Mary Reid<sup>1</sup>

4 <sup>1</sup>Northern Arizona University

## 5 **ABSTRACT**

6 The thermal regime of continental lithosphere plays a fundamental role in controlling the  
7 behavior of tectonic plates. In this work, we assess the thermal state of the North American upper  
8 mantle by combining shear-wave velocity models calculated using data from the EarthScope  
9 facility with empirically derived anelasticity models and basalt thermobarometry. We estimate  
10 the depth to the thermal lithosphere-asthenosphere boundary (LAB), defined as the intersection  
11 of a geotherm with the 1300° C adiabat. Results show lithospheric thicknesses across the  
12 contiguous US vary between ~40 km and > 200 km. The thinnest thermal lithosphere is observed  
13 in the tectonically active western US and the thickest lithosphere in the mid-continent. By  
14 combining geotherm estimates with solidus curves for peridotite, we show that a pervasive  
15 partial melt zone is common within the western US upper mantle and that partial melt is absent  
16 in the eastern and central US without significant metasomatism.

17

## 18 **PLAIN LANGUAGE SUMMARY**

19 The lithosphere, which is the upper most mechanical layer of the earth, makes up tectonic  
20 plates and can vary in thickness laterally. Thickness variations influence the location of  
21 volcanoes and where deformation occurs when forces act on the lithosphere. Lithospheric  
22 thicknesses can be estimated by examining the thermal properties of the uppermost mantle. We

23 integrate seismic observations and lab results to calculate temperatures for the upper mantle in  
24 the continental US and compare these to geochemical proxies for temperature. We then use these  
25 temperature results to estimate lithospheric thickness and map where melt is predicted within the  
26 upper mantle. Results show thin lithosphere and the presence of melt in the western US. Thicker  
27 lithosphere and an absence of melt are observed in the central and eastern US.

28

## 29 **INTRODUCTION**

30         The lithosphere-asthenosphere boundary (LAB) is a fundamental rheological boundary in  
31 the earth, separating the rigid lithosphere, which makes up the earth's tectonic plates, from  
32 ductile asthenosphere below. The decrease in seismic velocity with respect to depth often  
33 observed at this boundary is attributed to changes in rheology due to increased temperatures at  
34 depth, the presence of melt, and/or the transition from a chemically depleted mantle lithosphere  
35 to a more enriched asthenosphere [e.g. *Jordan, 1975; Fischer et al., 2010; Yuan and*  
36 *Romanowicz, 2010*]. Understanding the thermal state of the upper mantle is important for better  
37 understanding of the nature of the LAB in regions of both active tectonism and tectonic  
38 quiescence, and the behavior of lithosphere in general. To better understand the physical state of  
39 the mantle beneath North America, we utilize experimentally derived anelasticity data to convert  
40 shear velocities calculated using data from the EarthScope Transportable Array to temperatures  
41 and compare these results with basalt equilibration pressures and temperatures based on  
42 thermobarometry. We then present a new three-dimensional temperature model for the  
43 uppermost mantle beneath the continental US, which allows for a better understanding of upper-  
44 mantle rheology and the nature of the LAB across the continent.

45

## 46 **METHODOLOGY**

### 47 **Shear Velocities**

48 To calculate upper-mantle temperatures, we utilize a shear velocity model where  
49 velocities were calculated by inverting ambient noise and wave gradiometry data at periods  
50 between 8 and 150 seconds [Liu and Holt, 2015; Porter et al., 2016]. We use a linearized least  
51 squares inverse method where all phase velocity measurements are weighted equally to invert  
52 from phase velocity to shear velocity [Herrmann and Ammon, 2002]. The use of phase velocity  
53 measurements out to a period of 150 seconds allows for the calculation of a shear velocity model  
54 that extends down to ~200 km depth, which is deeper than many other existing surface wave  
55 measurements for the region allow for. In the shear velocity inversion, crustal and basin  
56 thicknesses are constrained using data from the Earthscope Automatic Receiver function Survey  
57 (EARS) [Crotwell and Owens, 2005], and the Laske and Masters [1997] global sediment  
58 thickness map.

### 59 **Seismic Temperature Calculations**

60 We use seismic velocities and pressure estimates to calculate temperatures for the upper  
61 mantle across the continental US. Within the mantle, the dominant control on seismic velocity is  
62 thought to be temperature, with the roles of factors such as composition, melt, and grain size  
63 debated and less constrained. Experimentally derived data from Isaak [1992] are used to  
64 calculate the effects of temperatures on the unrelaxed shear modulus for olivine. At high  
65 temperatures ( $> \sim 900^\circ \text{C}$ ) anelastic effects are pronounced and a linear relationship between  
66 increased temperature and anharmonic decreases in elastic moduli no longer holds [Goes et al.,  
67 2000; Cammarano et al., 2003; Faul and Jackson, 2005; Priestley and Mckenzie, 2006; Jackson  
68 et al., 2008; Jackson and Faul, 2010; McCarthy et al., 2011; Priestley and Mckenzie, 2013]. To

69 account for this, data from McCarthy et al. [2011] are used to relate velocities to temperature.  
70 Using these anharmonic and anelastic velocity/temperature relationships, we apply a Newton–  
71 Raphson iterative methodology to minimize the difference between predicted and observed  
72 velocities to calculate temperature as in Porter et al. [2019]. In our calculations, pressure is  
73 estimated using the crustal thickness model from Porter et al. [2016] and assuming a density of  
74  $2700 \text{ kg/m}^3$  for the crust. For calculating mantle densities, we follow the methodology of Goes et  
75 al. [2000], which accounts for the effects of pressure and temperature on upper mantle densities.  
76 Grain size is not well constrained within the mantle and may strongly influence the relationship  
77 between seismic velocities and temperatures, especially at elevated temperatures [*Jackson and*  
78 *Faul*, 2010; *McCarthy et al.*, 2011; e.g. *Dannberg et al.*, 2017]. As grain size may vary laterally  
79 and with depth within the upper mantle [e.g. *Karato and Wu*, 1993; *Behn et al.*, 2009], we  
80 assume a grain size of 1 mm in our estimates and show LAB estimates assuming grain size of 0.1  
81 mm in the Supplemental Data.

82 In our seismic temperature calculations, we assume that all velocity variations in the  
83 mantle are associated with temperature, which does not account for the effects of composition,  
84 melts, fluids, etc. on shear velocities. The relative effects of these factors on seismic velocity are  
85 variable and debated [*Anderson and Sammis*, 1970; *Karato*, 1995; *van der Lee*, 2002;  
86 *Cammarano et al.*, 2003; *Dunn and Forsyth*, 2003; *Artemieva et al.*, 2004; *Kreutzmann et al.*,  
87 2004; *Priestley and Mckenzie*, 2006; *Schutt and Leshner*, 2006; *Aizawa et al.*, 2007; *Schutt and*  
88 *Dueker*, 2008; *Karato*, 2010b; *Schutt and Leshner*, 2010; *Priestley and Mckenzie*, 2013;  
89 *Cammarano and Guerri*, 2017; *Cline et al.*, 2018]. While attributing all mantle seismic  
90 variations to temperature is a simplification of upper mantle conditions, this allows for a baseline

91 estimate of thermal conditions under the continent. For a more detailed discussion of these  
92 compositional assumptions and the methodology refer to Porter et al. [2019].

93 We use our seismically derived estimates of temperatures to calculate geotherms at every  
94 gridpoint within the shear velocity model. In order to estimate the thickness of the thermal  
95 lithosphere, we use the depth of the intersection of the 1300° C adiabat and seismically derived  
96 geotherms as a proxy for the location of the LAB (Figure 1). We also use these data to calculate  
97 the geothermal gradient in the upper mantle by measuring the vertical gradient of the estimated  
98 temperatures.

### 99 **Basalt Thermobarometry**

100 We calculate melt equilibrium pressure and temperatures using the major element  
101 thermobarometer described in Plank and Forsyth [2016]. Major oxide chemistries from basaltic  
102 rocks are downloaded from the EarthChem Portal ([www.earthchem.org/portal](http://www.earthchem.org/portal)) for all samples  
103 younger than 6 Ma within the western US and converted to molar percentages. The ratio of Fe<sup>3+</sup>  
104 to Fe<sup>2+</sup> is estimated assuming buffering of oxygen fugacity at the QFM buffer [*Kress and*  
105 *Carmichael*, 1991]. Whole rock compositions are converted to primary melt compositions by the  
106 sequential addition of olivine to obtain a melt in equilibration with Fo<sub>90</sub>, as in *Lee et al.* [2009].  
107 For our calculations, samples with less than 8% MgO, and/or 12% Al<sub>2</sub>O<sub>3</sub>, or those with  
108 unnormalized compositions of less than 97.5% by weight are deemed unlikely representative of  
109 near-primary mantle melts and were discarded. We estimate equilibrium P-T conditions  
110 assuming 1.5 wt % H<sub>2</sub>O in the melt because water measurements are not available for most  
111 samples. The 1.5% value was chosen as a rough average based on the water contents observed by  
112 Plank and Forsyth [2016], which ranged from 1-3.2%. To account for the range of possible  
113 magmatic water contents, the error bars in Figures 3, and 4 show the range of temperatures

114 (horizontal) and pressures (vertical) that are calculated when water contents were varied between  
115 0.5 wt % and 3 wt %. We compare our results to Plank and Forsyth [2016], who use vanadium to  
116 constrain oxygen fugacity and estimate  $\text{Fe}^{3+}$  to  $\text{Fe}^{2+}$  ratios. Resulting pressure-temperature  
117 estimate differences between our estimates and those of Plank and Forsyth [2016] are  $< 0.06$  GPa  
118 and  $< 14^\circ$  C when calculations were run for the same compositions assuming the same magmatic  
119 water contents.

### 120 **Seismic Mantle Melting Estimates**

121 In order to better understand the physical state of the upper mantle across the continent,  
122 we combine our seismic temperature estimates with experimental data that constrain solidi to  
123 map out where partial melt is present in the upper mantle across the contiguous US, assuming a  
124 peridotite upper mantle [Katz *et al.*, 2003]. The solidus was calculated for upper mantle depths  
125 assuming 75 ppm  $\text{H}_2\text{O}$ . We do not account for  $\text{CO}_2$  in these melting estimates, which has a  
126 considerably smaller effect than  $\text{H}_2\text{O}$  and is negligible for melt equilibration pressures  $< 2$  GPa  
127 [Plank and Forsyth, 2016]. At temperatures above the solidus, the presence of partial melt is  
128 expected within the upper mantle, which would lower seismic velocities, and lead to an  
129 overestimation of seismically derived temperatures. Because of the uncertainty in this  
130 relationship, instead of estimating melt fractions based on temperature, we subtract solidus  
131 temperatures from our seismically derived temperatures estimates. This allows us to predict  
132 where partial melting is expected within the upper mantle.

133 The value of 75 ppm water was selected as a wet average for “damp” upper mantle.  
134 Previous geophysical estimates are consistent with 0-100 ppm water within the upper mantle  
135 outside of subduction zones [Khan and Shankland, 2010]. In actuality, hydration is likely  
136 variable both vertically and horizontally within the upper mantle [Karato, 2010a]. At a

137 continental scale, higher water contents are likely present in the western US than in the eastern  
138 and central parts of the country due to the recent history of subduction across the region  
139 [Humphreys *et al.*, 2003]. At a finer scale, hydration is likely variable regionally due to  
140 variations in geologic settings including lateral heterogeneity in slab dehydration [Dixon *et al.*,  
141 2004], the extent of fluid introduction into the upper mantle during continental formation  
142 [Selverstone *et al.*, 1999], and post-formational processes such as cratonic rejuvenation [Rudnick  
143 *et al.*, 1998; Carlson, 2005; Griffin *et al.*, 2009; Lee *et al.*, 2011; Eeken *et al.*, 2018].  
144 Compounding this uncertainty in the efficacy of hydration, mantle dehydration due to heating  
145 and related volcanism is likely inconsistent across the continent. The results reported here should  
146 help guide where expanded constraints on mantle hydration are imperative for better constraining  
147 the thermal and viscosity structure of the upper mantle.

148

## 149 **RESULTS**

150 Results of the seismic temperature calculations show large variations in the thermal  
151 regimes within the upper mantle across the continental US. As expected, cooler temperatures are  
152 observed throughout the uppermost mantle within the tectonically quiescent eastern and central  
153 US relative to tectonically active western US (Figures 1, 2, and 3). The hottest temperatures and  
154 thinnest lithosphere within the western US correspond to regions of recent extension and/or  
155 hypothesized mantle upwelling.

156 Melt thermobarometry estimates are primarily for generation of recently emplaced basalts  
157 in the Snake River Plain, the Basin and Range/Colorado Plateau margins, and the Cascade Arc  
158 (Figure 3). We show results from all samples though a few give erroneous results that result in  
159 pressure estimates less than that at the Moho (e.g. the low-P CP sample in Figure 3). Pressure-

160 temperature estimates from the Snake River Plain and Colorado Plateau generally exhibit  
161 relatively high equilibrium temperatures and deeper depths than those within the Cascades, even  
162 before the higher water contents likely present under the Cascades are considered (Figures 3 and  
163 4). Our seismically derived thermal estimates generally agree well with the melt  
164 thermobarometry results (Figures 3 and 4). Where seismic geotherms do not agree with  
165 thermobarometry estimates, it is often in places where sharp lateral changes in upper mantle  
166 temperature occur (e.g. the edges of the Snake River Plain). In the seismic model, these  
167 boundaries may appear gradational due to smoothing. At pressures  $> 2$  GPa, the Plank and  
168 Forsyth [2016] estimates plot closer to the  $1300^{\circ}$  C adiabat, likely because of the higher water  
169 contents in those samples ( $> 2$  wt. % for many) than the fixed value used here. When we assume  
170 greater degrees of hydration (indicated by the horizontal error bars in Figures 3 and 4) the  
171 temperature estimates are relatively consistent between our estimates and Plank and Forsyth  
172 [2016]. In comparing our seismic estimates of temperature to basalt equilibrium estimates, it is  
173 apparent that volatiles are required to produce melts at depth  $> 2$  GPa, as few seismically derived  
174 geotherms show conditions hot enough to match PT estimates for basalts containing 1.5 wt %  
175 water. This is consistent with hydration of the upper mantle beneath the Colorado Plateau and  
176 parts of the western US due to the dehydration of a flat-slab during present beneath the region  
177 during the late Cretaceous/Early Cenozoic.

178         In our seismic results, thinned thermal lithosphere ( $< 100$  km thick) is observed across  
179 much of the Basin and Range Province, beneath the Snake River Plain/Yellowstone hotspot  
180 trace, and in the backarc of the Cascade Mountains in Washington and Oregon (Figures 1 and 2).  
181 The thickest lithosphere ( $> 180$  km thick) is observed in the central US where the cratonic core  
182 of the continent is located. The shear model used to derive temperatures only has resolution

183 down to ~200 km depth; as such, estimates of ~200 km are likely a minimum thickness for  
184 thermal lithosphere in cratonic regions and are not well-constrained. Intermediate lithospheric  
185 thicknesses are observed along the eastern margin of the continent where rifting occurred during  
186 the opening of the Atlantic Ocean in the Jurassic. A west-east cross section of temperature across  
187 the continent highlights these variations in temperatures and depth to the thermal LAB (Figure  
188 2). These results agree with body-wave tomography results which show a high-velocity keel  
189 beneath the cratonic region of North America that extends down to ~200 km depth [*Schmandt*  
190 *and Lin, 2014*], and with previous temperature estimates for the uppermost mantle [*Goes and van*  
191 *der Lee, 2002; Schutt et al., 2018*]. Thermal estimates also show slightly increased  
192 temperatures/thinned thermal lithosphere along the eastern seaboard in the vicinity of New  
193 England and western Virginia (Figure 1). These high temperature zones align with areas where  
194 recent tectonism has been proposed [*van der Lee et al., 2008; Mazza et al., 2014; Schmandt and*  
195 *Lin, 2014; Menke et al., 2016*].

196         Zones of partial melting were mapped by identifying regions where seismically derived  
197 geotherms exceed the predicted pressure-dependent solidus for peridotite with 75 ppm water.  
198 Figure 3 shows the maximum difference between the seismically derived temperature estimates  
199 and the peridotite solidus at all depths for gridpoints using the parameterization of Katz et al.  
200 [2003]. Results show that partial melt is likely present within the mantle across much of the  
201 western US, where thin lithosphere is observed, and absent within the eastern and central US  
202 where the lithosphere is thicker.

203         Within the western US, the LAB may be defined by a zone of significant partial melting,  
204 which would lower both mantle viscosity and, if enough partial melt were present, seismic  
205 velocities. This sharp velocity gradient would result in a relatively sharp LAB conversion in

206 receiver functions. Basaltic volcanism in the western US is most commonly observed within the  
207 Basin and Range province where widespread extension, large-scale mantle upwelling, and small-  
208 scale convection have been proposed, and within the Snake River Plain where mantle upwelling  
209 associated with the Yellowstone hotspot is driving volcanism. In the eastern and central US,  
210 melts are predicted to be absent at the LAB for mantle containing 75 ppm water and the  
211 transition from lithosphere to asthenosphere may involve a gradual transition in viscosity.

212 A cross section of geothermal gradient highlights the varying temperature regimes within  
213 the upper mantle across the continental US (Figure 2). Higher gradients ( $> 2^\circ \text{C/km}$ ) are  
214 observed within the thermally defined ( $< 1300^\circ \text{C}$ ) lithospheric mantle than within areas mapped  
215 as asthenosphere ( $> 1300^\circ \text{C}$ ). These variations are consistent with conduction as the dominant  
216 mechanism of heat transfer in the lithosphere and advection or convection as the dominant  
217 mechanisms of heat transfer in the asthenosphere (Figure 2). In a few locations in the western  
218 US, low geothermal gradients are observed in regions where observed mantle temperatures are  
219 below  $1300^\circ \text{C}$ . Low gradients in these regions can be explained by uncertainty in the model  
220 and/or the presence of partial melt in these regions (Figure 2), which would likely allow for  
221 advective heat transfer. It is also possible that partial melting of these regions may lower the  
222 viscosity of the mantle enough for convective heat transfer to occur. In these cases, the  $1300^\circ \text{C}$   
223 isotherm would likely be an inaccurate proxy for rheological lithospheric thickness.

224

## 225 **DISCUSSION**

### 226 **Nature of the Lithosphere-Asthenosphere Boundary**

227 In this work, we show that upper-mantle thermal conditions within much of the western  
228 US are near or above the solidus for partially hydrated peridotite (Figure 2), consistent with the

229 hypothesis that partial melt may play a role in controlling the thickness of mantle lithosphere in  
230 this region [Hopper and Fischer, 2018]. The presence or absence of partial melt in the upper  
231 mantle may influence how the rheological LAB, which separates viscous lithosphere from the  
232 lower viscosity asthenosphere [e.g. Fischer et al., 2010], is observed seismically. In the western  
233 US, Sp receiver function work shows a laterally extensive high-amplitude negative conversion  
234 interpreted as the LAB, which can be explained by the presence of partial melt at this boundary  
235 and an abrupt boundary between lithosphere and asthenosphere [Abt et al., 2010; Hopper and  
236 Fischer, 2018]. In the central cratonic US, mid-lithosphere seismic discontinues are observed in  
237 receiver functions, however, there is no conversion that can be clearly associated with the LAB.  
238 This lack of a clear boundary is consistent with a gradual transition from lithosphere to lower-  
239 viscosity asthenosphere in these regions [Abt et al., 2010; Hopper and Fischer, 2018]. Within the  
240 eastern US, receiver function amplitudes are consistent with partial melt at the LAB [Hopper and  
241 Fischer, 2018], however, we do not observe temperatures high enough to result in melting  
242 without volatile addition (Figure 4).

243         Based on our seismically derived temperature estimates and the timing of tectonism,  
244 extensive upper mantle melting is expected only in areas with recent thermotectonic activity.  
245 This is highlighted in Figure 4 which shows geotherms taken from our model at gridpoints  
246 located at 1° latitude and longitude intervals. These geotherms are shaded using the  
247 thermotectonic age model of Porter et al. [2019], which is based on dating of surface volcanic  
248 rocks. Of these geotherms, the 75 ppm solidus is only exceeded by those with nearby young (<  
249 10 Ma) volcanism. Figure 4 highlights the importance of thinned lithosphere in the occurrence of  
250 melting. In all but the hottest geotherms, melting with moderate hydration can only occur at  
251 relatively shallow depths (< ~100 km) within the mantle. Given this constraint, partial melt is

252 likely to define and yield a sharp LAB, observable in receiver functions, within regions of  
253 relatively thin and recently modified lithosphere or in areas carbonated and/or hydrated by  
254 extensive metasomatism.

255         Carbon dioxide-assisted melting is hypothesized as a mechanism for controlling the LAB  
256 by lowering the peridotite solidus in cratonic regions [Tharimena *et al.*, 2017]. The presence of  
257 carbon dioxide (in addition to water) can significantly lower the peridotite solidus [Foley *et al.*,  
258 2009] and has been hypothesized as especially important for producing small-degree melting at  
259 depth within the mantle beneath mid-ocean ridges [Dasgupta and Hirschmann, 2006]. Our  
260 results are consistent with temperature exceeding the carbonated peridotite solidus at depths  
261 between 100-180 km in cratonic regions. However, this depth is shallower than our thermally  
262 derived LAB under the cratonic region of the US. Modeling work shows that, if the LAB is  
263 defined rheologically, the viscosity contrast at this boundary is between 3 and 10 orders of  
264 magnitude [Doglioni *et al.*, 2011; Rolf *et al.*, 2018]. To produce a velocity contrast of this  
265 magnitude between a solid and partially molten rock, a melt fraction,  $\phi$ ,  $> 0.2$  is required  
266 [Kohlstedt and Hansen, 2015]. Such a melt fraction, even if arising from magma pooling, would  
267 require widespread carbonization and/or hydration of the upper mantle to produce an extensive  
268 region with this degree of melting. Because of this, we prefer a thermal rather than melt-related  
269 explanation for the LAB under the cratonic US that results in a gradational boundary.

270

## 271 **CONCLUSIONS**

272         Results from this work highlight the varied thermal states of the upper mantle across the  
273 continental US and shed insight into the nature of the lithosphere-asthenosphere boundary within  
274 the region. In our measurements, we observe hotter temperatures and zones of extensive melting

275 in the western US that are absent in the central and eastern US. These zones of mapped melts  
276 align well with recently emplaced basalts at the surface. Melt within the tectonically active  
277 western US likely defines the LAB while this is less likely in cratons where melts would only  
278 form in zones of concentrated metasomatism.

279

## 280 **ACKNOWLEDGMENTS**

281 This work was funded by NSF Award EAR-1829520. Seismic data were collected as part  
282 of the EarthScope experiment and downloaded from the IRIS DMC.

283

## 284 **DATA AVAILABILITY STATEMENT**

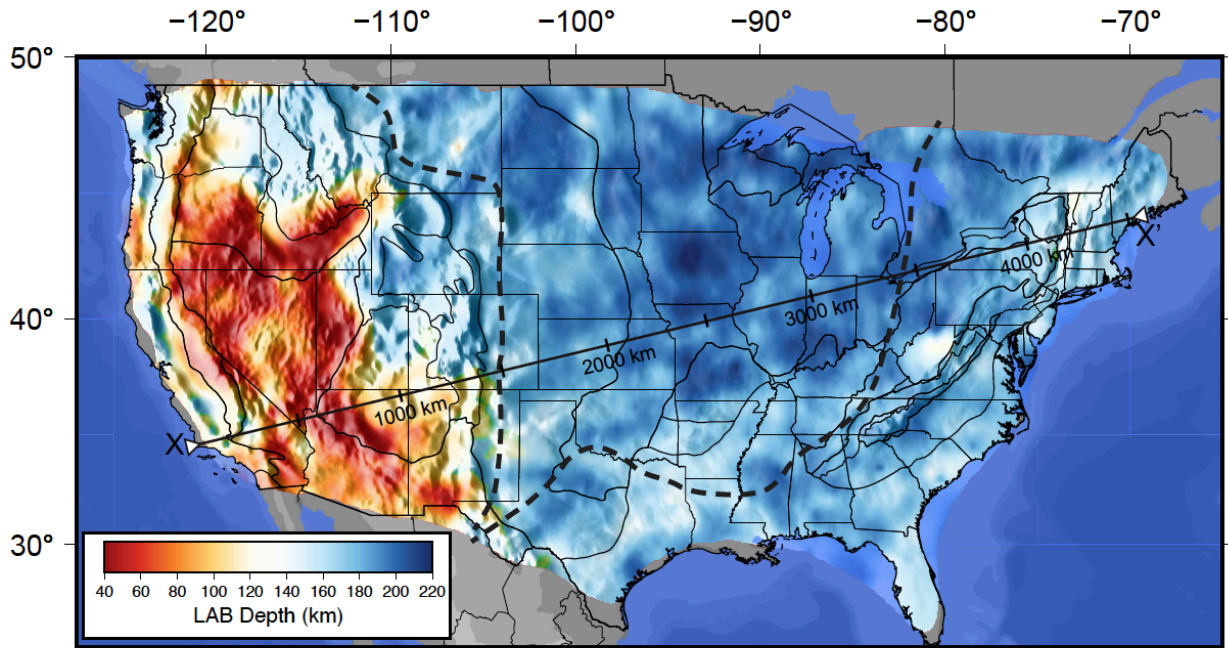
285 Data from the TA network were made freely available as part of the EarthScope USArray  
286 facility, operated by Incorporated Research Institutions for Seismology (IRIS) and supported by  
287 the National Science Foundation, under Cooperative Agreements EAR-1261681. No new data  
288 were collected as part of this work, the seismic data used can be accessed at:

289 <https://ds.iris.edu/ds/nodes/dmc/>. The geochemical data are available at:

290 [www.earthchem.org/portal](http://www.earthchem.org/portal).

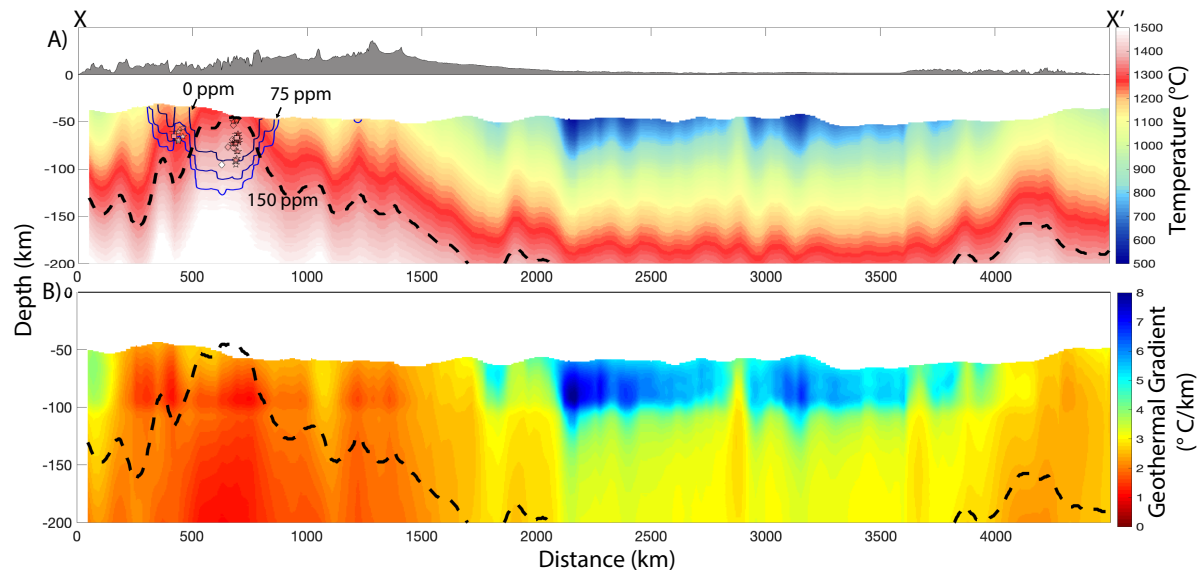
291

292 **FIGURE CAPTIONS**



293

294 Figure 1. Map of depth to the 1300° C adiabat, which is interpreted as the base of the thermal  
295 lithosphere. Bold lines are physiographic provinces modified from Fenneman [1917]. Thick  
296 dashed line denotes the Grenville Front and eastern limit of Cordilleran strain [DeCelles, 2004;  
297 *Whitmeyer and Karlstrom, 2007*]. Line X-X' shows the location of the cross section in Figure 2.  
298 Hill shade shows topography.

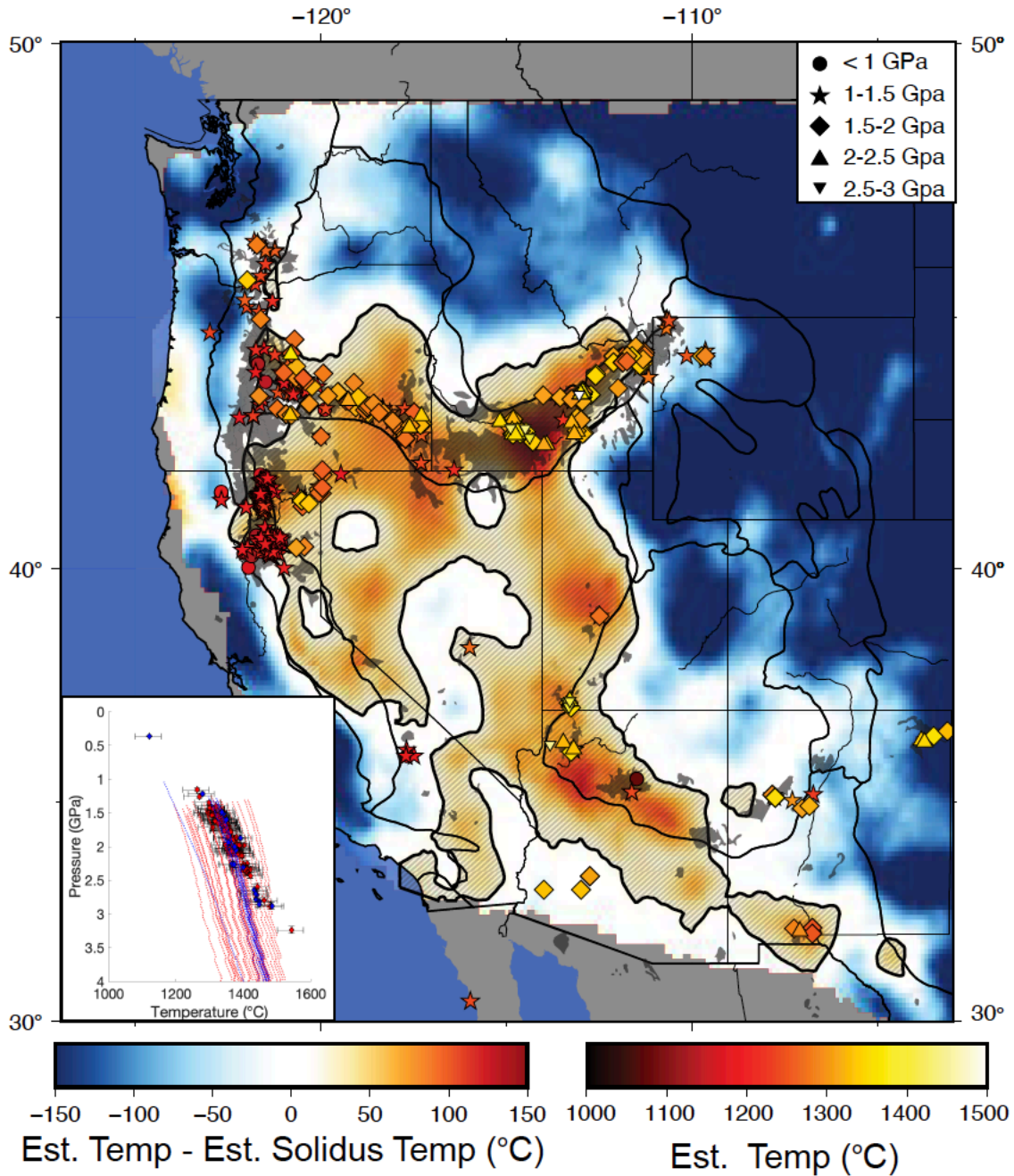


299

300 Figure 2. Thermal profiles along line X-X'. Panel A shows seismically derived upper mantle  
 301 temperature estimates. The dashed black line is where the modeled temperatures reach the 1300°  
 302 C adiabat, which we interpret as the thermal LAB. The thin blue lines are the estimated solidi  
 303 assuming anhydrous conditions (dark blue), 75 ppm water (medium blue), and 150 ppm water  
 304 (light blue). Melt is expected in the regions above these curves. Diamond are basalt melt  
 305 equilibrium P-T conditions from this study. Fill colors indicate temperature estimates. Stars are  
 306 P-T conditions from Plank and Forsyth [2016] and squares are from Klöcking [2018]. Panel B  
 307 shows smoothed geothermal gradient for cross section X-X'. Higher geothermal gradients are  
 308 observed in cratonic areas with thick lithosphere relative to areas of thinned lithosphere. Dashed  
 309 line is the thermal LAB.

310

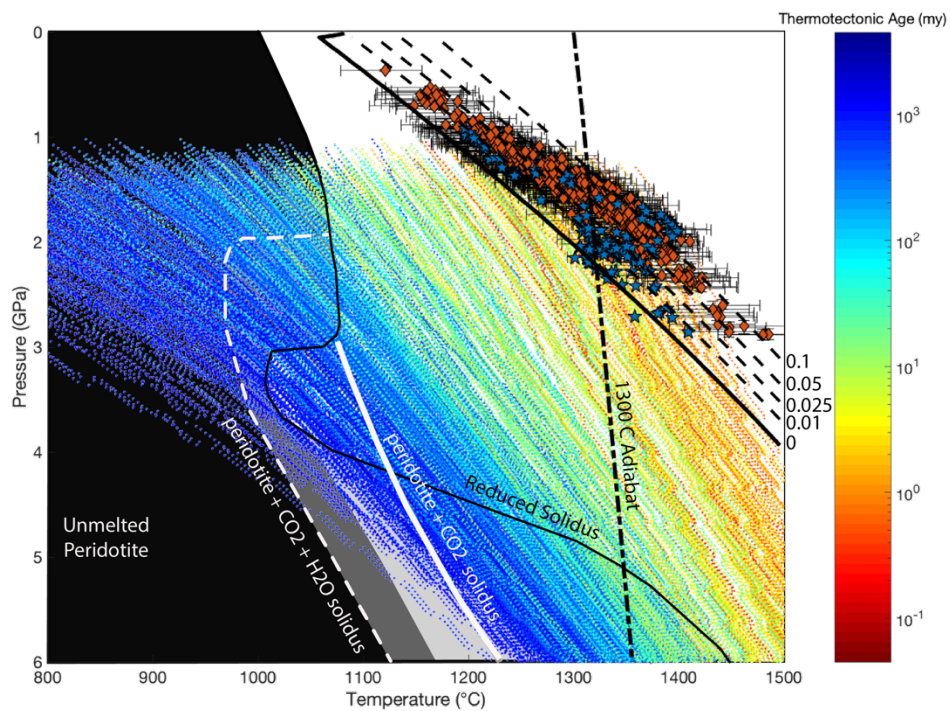
311



312

313 Figure 3. Map showing maximum temperature difference between seismically estimated mantle  
 314 temperatures ( $T_{est}$ ) and the temperature of the solidus ( $T_{sol}$ ) for partially hydrated (75 ppm)  
 315 peridotite at all depths for each gridpoint (i.e.  $\max(T_{est}(d) - T_{sol}(d))$  where  $d$  is every depth in the  
 316 model). Melt is expected in areas where positive values are observed. Plotted symbols indicate

317 the location, temperature and pressure of melt thermobarometry data. Black regions are mapped  
318 Pliocene and younger volcanic units from the Decade of North American Geology: Geologic  
319 Map of North America [Reed *et al.*, 2005]. Physiographic provinces modified from Fenneman  
320 [1917]. Inset shows the melt equilibrium estimates (diamonds) and the closest seismically  
321 derived geotherm (dotted lines) from the Colorado Plateau (blue) and Snake River Plain (red).  
322 The spread in Snake River Plain seismic geotherms is due to the sharp boundaries of the  
323 province.



324  
325 Figure 4. Pressure-temperature plots of seismic and basalt melt equilibrium data. Dotted lines are  
326 seismically derived geotherms for the continental US taken at 1° intervals. Geotherms colors are  
327 based on thermotectonic age for their location using the model of Porter *et al.* [2019]. Orange  
328 diamonds are basalt melt equilibrium P-T conditions from this study. Error bars show the effects  
329 of varying water contents between 0.5 wt % and 3 wt % on temperature (horizontal) and pressure  
330 (vertical) for each sample. Blue stars are P-T conditions from Plank and Forsyth [2016]. Solid

331 black line is the solidus and labeled dashed contour lines are melt fractions based on Katz et al.  
332 [2003] for 75 ppm water in the upper mantle. The sub-vertical dashed black line is the 1300° C  
333 adiabat. Background shading and additional lines are CO<sub>2</sub> solidi modified from Foley et al.  
334 [2009].

335

336

337

### 338 REFERENCES CITED

339

340 Abt, D. L., K. M. Fischer, S. W. French, H. A. Ford, H. Yuan, and B. Romanowicz (2010),  
341 North American lithospheric discontinuity structure imaged by Psand Spreceiver functions, *J*  
342 *Geophys Res-Solid*, 115(B9), B09301, doi:10.1029/2009JB006914.

343 Aizawa, Y., A. Barnhoorn, U. H. Faul, J. D. Fitz Gerald, I. Jackson, and I. Kovacs (2007),  
344 Seismic Properties of Anita Bay Dunite: an Exploratory Study of the Influence of Water, *J*  
345 *Petrol*, 49(4), 841–855, doi:10.1093/petrology/egn007.

346 Anderson, D. L., and C. Sammis (1970), Partial melting in the upper mantle, *PEPI*, 3, 41–50,  
347 doi:10.1016/0031-9201(70)90042-7.

348 Artemieva, I. M., M. Billien, J.-J. L ev eque, and W. D. Mooney (2004), Shear wave velocity,  
349 seismic attenuation, and thermal structure of the continental upper mantle, *GeoJI*, 157(2),  
350 607–628, doi:10.1111/j.1365-246X.2004.02195.x.

351 Behn, M. D., G. Hirth, and J. R. Elsenbeck II (2009), Implications of grain size evolution on the  
352 seismic structure of the oceanic upper mantle, *E&PSL*, 282(1-4), 178–189,  
353 doi:10.1016/j.epsl.2009.03.014.

354 Cammarano, F., and M. Guerri (2017), Global thermal models of the lithosphere, *GeoJI*, 210(1),  
355 56–72, doi:10.1093/gji/ggx144.

356 Cammarano, F., S. Goes, P. Vacher, and D. Giardini (2003), Inferring upper-mantle temperatures  
357 from seismic velocities, *PEPI*, 138(3-4), 197–222, doi:10.1016/S0031-9201(03)00156-0.

358 Carlson, R. W. (2005), Physical, chemical, and chronological characteristics of continental  
359 mantle, *Rev Geophys*, 43(1), 1–24, doi:10.1029/2004RG000156.

- 360 Cline, C. J., U. H. Faul, E. C. David, A. J. Berry, and I. Jackson (2018), Redox-influenced  
361 seismic properties of upper- mantle olivine, *Nature*, 555(7696), 355–358,  
362 doi:10.1038/nature25764.
- 363 Crotwell, H. P., and T. J. Owens (2005), Automated receiver function processing, *Seismological*  
364 *Research Letters*, 76(6), 702–709.
- 365 Dannberg, J., Z. Eilon, U. Faul, R. Gassmöller, P. Moulik, and R. Myhill (2017), The importance  
366 of grain size to mantle dynamics and seismological observations, *Geochemistry, Geophysics,*  
367 *Geosystems*, 18(8), 3034–3061, doi:10.1002/2017GC006944.
- 368 Dasgupta, R., and M. M. Hirschmann (2006), Melting in the Earth's deep upper mantle caused by  
369 carbon dioxide, *Nature*, 440(7084), 659–662, doi:10.1038/nature04612.
- 370 DeCelles, P. G. (2004), Late Jurassic to Eocene evolution of the Cordilleran thrust belt and  
371 foreland basin system, western USA, *AmJS*, 304(2), 105.
- 372 Dixon, J. E., T. H. Dixon, D. R. Bell, and R. Malservisi (2004), Lateral variation in upper mantle  
373 viscosity: role of water, *E&PSL*, 222(2), 451–467, doi:10.1016/j.epsl.2004.03.022.
- 374 Doglioni, C., A. Ismail-Zadeh, G. Panza, and F. Riguzzi (2011), Lithosphere–asthenosphere  
375 viscosity contrast and decoupling, *PEPI*, 189(1-2), 1–8, doi:10.1016/j.pepi.2011.09.006.
- 376 Dunn, R. A., and D. W. Forsyth (2003), Imaging the transition between the region of mantle melt  
377 generation and the crustal magma chamber beneath the southern East Pacific Rise with  
378 short-period Love waves, *JGR*, 108(B7), 641, doi:10.1029/2002JB002217.
- 379 Eeken, T., S. Goes, H. A. Pedersen, N. A. E. A. Planetary, 2018 (2018), Seismic evidence for  
380 depth-dependent metasomatism in cratons, *EPSL*, 491, 148–159,  
381 doi:10.1016/j.epsl.2018.03.018.
- 382 Faul, U., and I. Jackson (2005), The seismological signature of temperature and grain size  
383 variations in the upper mantle, *E&PSL*, 234(1-2), 119–134, doi:10.1016/j.epsl.2005.02.008.
- 384 Fenneman, N. M. (1917), Physiographic divisions of the United States, *Proceedings of the*  
385 *National Academy of Science of the United States of America*, 1(3), 17–22,  
386 doi:10.1073/pnas.3.1.17.
- 387 Fischer, K. M., H. A. Ford, D. L. Abt, and C. A. Rychert (2010), The lithosphere-asthenosphere  
388 boundary, *Annu. Rev. Earth Planet. Sci.*, 38(1), 551–575, doi:10.1146/annurev-earth-  
389 040809-152438.
- 390 Foley, S. F., G. M. Yaxley, A. Rosenthal, S. Buhre, E. S. Kiseeva, R. P. Rapp, and D. E. Jacob  
391 (2009), The composition of near-solidus melts of peridotite in the presence of CO<sub>2</sub> and H<sub>2</sub>O  
392 between 40 and 60 kbar, *Litho*, 112(S1), 274–283, doi:10.1016/j.lithos.2009.03.020.

- 393 Goes, S., R. Govers, and P. Vacher (2000), Shallow mantle temperatures under Europe from P  
394 and Swave tomography, *J Geophys Res-Solid*, 105(B5), 11153–18,  
395 doi:10.1029/1999JB900300.
- 396 Goes, S. and van der Lee, S., (2002), Thermal structure of the North American uppermost mantle  
397 inferred from seismic tomography. *Journal of Geophysical Research: Solid Earth*, 107(B3).  
398
- 399 Griffin, W. L., S. Y. O'Reilly, J. C. Afonso, and G. C. Begg (2009), The Composition and  
400 Evolution of Lithospheric Mantle: a Re-evaluation and its Tectonic Implications, *J Petrol*.
- 401 Herrmann, R. B., and C. J. Ammon (2002), Computer Programs in Seismology–Surface Waves,  
402 Receiver Functions and Crustal Structure, *St. Louis University*.
- 403 Hopper, E., and K. M. Fischer (2018), The Changing Face of the Lithosphere-Asthenosphere  
404 Boundary: Imaging Continental Scale Patterns in Upper Mantle Structure Across the  
405 Contiguous U.S. With Sp Converted Waves, *Geochem. Geophys. Geosyst.*, 19(8), 2593–  
406 2614, doi:10.1029/2018GC007476.
- 407 Humphreys, E., E. Hessler, K. Dueker, G. L. Farmer, E. Erslev, and T. Atwater (2003), How  
408 Laramide-age hydration of North American lithosphere by the Farallon slab controlled  
409 subsequent activity in the western United States, *International Geology Review*, 45(7), 575–  
410 595.
- 411 Isaak, D. G. (1992), High-temperature elasticity of iron-bearing olivines, *JGR*, 97(B2), 1871–  
412 1885.
- 413 Jackson, I., and U. H. Faul (2010), Grainsize-sensitive viscoelastic relaxation in olivine: Towards  
414 a robust laboratory-based model for seismological application, *PEPI*, 183(1-2), 151–163,  
415 doi:10.1016/j.pepi.2010.09.005.
- 416 Jackson, J., D. Mckenzie, K. Priestley, and B. Emmerson (2008), New views on the structure and  
417 rheology of the lithosphere,, *165*, 453–465.
- 418 Jordan, T. H. (1975), The continental tectosphere, *Rev Geophys*, 13(3), 1–12,  
419 doi:10.1029/RG013i003p00001.
- 420 Karato, S. (1995), Effects of Water on Seismic-Wave Velocities in the Upper-Mantle,  
421 *Proceedings of the Japan Academy Series B-Physical and Biological Sciences*, 71(2), 61–66.
- 422 Karato, S. I. (2010a), Mapping water content in the upper mantle, in *Volcanism and Subduction:*  
423 *The Kamchatka Region*, vol. 138, pp. 135–152, American Geophysical Union, Washington,  
424 D. C.
- 425 Karato, S. I. (2010b), Rheology of the deep upper mantle and its implications for the  
426 preservation of the continental roots: A review, *Tectonophysics*, 481(1-4), 82–98,  
427 doi:10.1016/j.tecto.2009.04.011.

- 428 Karato, S. I., and P. Wu (1993), Rheology of the Upper Mantle: A Synthesis, *Sci*, 260(5109),  
429 771–778.
- 430 Katz, R. F., Geochemistry, M. S., Katz, R. F., 2003, M. Spiegelman, M. Spiegelman, and C. H.  
431 Langmuir (2003), A new parameterization of hydrous mantle melting, *Geochem Geophys*  
432 *Geosy*, 4, 19, doi:10.1029/2002GC000433.
- 433 Khan, A., and T. J. Shankland (2010), A geophysical perspective on mantle water content and  
434 melting: Inverting electromagnetic sounding data using laboratory-based electrical  
435 conductivity profiles, *E&PSL*, 317-318, 1–17, doi:10.1016/j.epsl.2011.11.031.
- 436 Klöcking, M., N. J. White, J. MacLennan, D. Mckenzie, and J. G. Fitton (2018), Quantitative  
437 Relationships Between Basalt Geochemistry, Shear Wave Velocity, and Asthenospheric  
438 Temperature Beneath Western North America, *Geochem. Geophys. Geosyst.*, 19(9), 3376–  
439 3404, doi:10.1029/2018GC007559.
- 440 Kohlstedt, D. L., and L. N. Hansen (2015), Constitutive Equations, Rheological Behavior, and  
441 Viscosity of Rocks, in *Constitutive equations, rheological behavior, and viscosity of rocks*,  
442 pp. 441–472, Elsevier.
- 443 Kress, V. C., and I. S. Carmichael (1991), The compressibility of silicate liquids containing  
444 Fe<sub>2</sub>O<sub>3</sub> and the effect of composition, temperature, oxygen fugacity and pressure on their  
445 redox states, *Contrib Mineral Petr*, 108(1-2), 82–92.
- 446 Kreuzmann, A., H. Schmeling, A. Junge, T. Ruedas, G. Marquart, and I. T. Bjarnason (2004),  
447 Temperature and melting of a ridge-centred plume with application to Iceland. Part II:  
448 Predictions for electromagnetic and seismic observables, *GeoJI*, 159(3), 1097–1111,  
449 doi:10.1111/j.1365-246X.2004.02397.x.
- 450 Laske, G., and G. Masters (1997), A global digital map of sediment thickness, *Eos Trans. AGU*,  
451 78(F483).
- 452 Lee, C.-T. A., P. Luffi, and E. J. Chin (2011), Building and Destroying Continental Mantle,  
453 *Annu. Rev. Earth Planet. Sci.*, 39(1), 59–90, doi:10.1146/annurev-earth-040610-133505.
- 454 Lee, C.-T. A., P. Luffi, T. Plank, H. Dalton, and W. P. Leeman (2009), Constraints on the depths  
455 and temperatures of basaltic magma generation on Earth and other terrestrial planets using  
456 new thermobarometers for mafic magmas, *E&PSL*, 279(1-2), 20–33,  
457 doi:10.1016/j.epsl.2008.12.020.
- 458 Liu, Y., and W. E. Holt (2015), Wave gradiometry and its link with Helmholtz equation  
459 solutions applied to USArray in the eastern US, *J. Geophys. Res. Solid Earth*,  
460 doi:10.1002/(ISSN)2169-9356.
- 461 Mazza, S. E., E. Gazel, E. A. Johnson, M. J. Kunk, R. McAleer, J. A. Spotila, M. Bizimis, and D.  
462 S. Coleman (2014), Volcanoes of the passive margin: The youngest magmatic event in  
463 eastern North America, *Geol*, 42(6), 483–486, doi:10.1130/G35407.1.

- 464 McCarthy, C., Y. Takei, and T. Hiraga (2011), Experimental study of attenuation and dispersion  
465 over a broad frequency range: 2. The universal scaling of polycrystalline materials, *JGR*,  
466 *116*(B9), 3893, doi:10.1029/2011JB008384.
- 467 Menke, W., P. Skryzalin, V. Levin, and T. Harper (2016), The Northern Appalachian Anomaly:  
468 A modern asthenospheric upwelling, *GRL*, *43*(19), 10,173–10,179,  
469 doi:10.1002/2016GL070918.
- 470 Plank, T., and D. W. Forsyth (2016), Thermal structure and melting conditions in the mantle  
471 beneath the Basin and Range province from seismology and petrology, *Geochem. Geophys.*  
472 *Geosyst.*, *17*(4), 1312–1338, doi:10.1002/2015GC006205.
- 473 Porter, R. C., S. van der Lee, and S. J. Whitmeyer (2019), Synthesizing EarthScope data to  
474 constrain the thermal evolution of the continental U.S. lithosphere, *Geosphere*, *15*(6), 1722–  
475 1737, doi:10.1130/GES02000.1.
- 476 Porter, R., Y. Liu, Y. Liu, W. E. Holt, and W. E. Holt (2016), Lithospheric records of orogeny  
477 within the continental US, *GeoRL*, *43*(1), 144–153, doi:10.1002/2015GL066950.
- 478 Priestley, K., and D. Mckenzie (2006), The thermal structure of the lithosphere from shear wave  
479 velocities, *E&PSL*, *244*(1-2), 285–301.
- 480 Priestley, K., and D. Mckenzie (2013), The relationship between shear wave velocity,  
481 temperature, attenuation and viscosity in the shallow part of the mantle, *E&PSL*, *381*, 78–91,  
482 doi:10.1016/j.epsl.2013.08.022.
- 483 Reed, J. C., B. E. Tucholke, and J. O. Wheeler (2005), Decade of North American Geology:  
484 Geologic Map of North America: Perspectives and Explanation,
- 485 Rolf, T., F. A. Capitanio, and P. J. Tackley (2018), Constraints on mantle viscosity structure  
486 from continental drift histories in spherical mantle convection models, *Tectonophysics*,  
487 *746*(C), 339–351, doi:10.1016/j.tecto.2017.04.031.
- 488 Rudnick, R. L., W. F. McDonough, and R. J. O'Connell (1998), Thermal structure, thickness and  
489 composition of continental lithosphere, *Chemical Geology*, *145*(3-4), 395–411,  
490 doi:10.1016/S0009-2541(97)00151-4.
- 491 Schmandt, B., and F.-C. Lin (2014), P and S wave tomography of the mantle beneath the United  
492 States, *GeoRL*, *41*, 1–8, doi:10.1002/(ISSN)1944-8007.
- 493 Schutt, D. L., A. R. Lowry, and J. S. Buehler (2018), Moho temperature and mobility of lower  
494 crust in the western United States, *Geol*, 1–4, doi:10.1130/G39507.1.
- 495 Schutt, D. L., and C. E. Leshner (2006), Effects of melt depletion on the density and seismic  
496 velocity of garnet and spinel lherzolite, *JGR*, *111*(B5), B05401, doi:10.1029/2003JB002950.

497 Schutt, D. L., and C. E. Lesher (2010), Compositional trends among Kaapvaal Craton garnet  
498 peridotite xenoliths and their effects on seismic velocity and density, *E&PSL*, 300(3-4), 367–  
499 373, doi:10.1016/j.epsl.2010.10.018.

500 Schutt, D. L., and K. Dueker (2008), Temperature of the plume layer beneath the Yellowstone  
501 hotspot, *Geol*, 36(8), 623–4, doi:10.1130/G24809A.1.

502 Selverstone, J., A. Pun, and K. C. Condie (1999), Xenolithic evidence for Proterozoic crustal  
503 evolution beneath the Colorado Plateau, *Geol Soc Am Bull*, 111(4), 590–606,  
504 doi:10.1130/0016-7606(1999)111<0590:XEFPCE>2.3.CO;2.

505 Tharimena, S., C. Rychert, and N. Harmon (2017), A unified continental thickness from  
506 seismology and diamonds suggests a melt-defined plate, *Sci*, 357(6351), 580–583.

507 van der Lee, S. (2002), High-resolution estimates of lithospheric thickness from Missouri to  
508 Massachusetts, USA, *E&PSL*, 203(1), 15–23.

509 van der Lee, S., K. Regenauer-Lieb, and D. A. Yuen (2008), The role of water in connecting past  
510 and future episodes of subduction, *E&PSL*, 273(1-2), 15–27, doi:10.1016/j.epsl.2008.04.041.

511 Whitmeyer, S. J., and K. E. Karlstrom (2007), Tectonic model for the Proterozoic growth of  
512 North America, *Geosphere*, 3(4), 220.

513 Yuan, H., and B. Romanowicz (2010), Lithospheric layering in the North American craton,  
514 *Nature*, 466(7310), 1063–1068, doi:10.1038/nature09332.

515

516

517

518

519

520

521

522

523

524

525